Journal of Medicinal Chemistry

Article

pubs.acs.org/jmc

Structure–Activity Relationships and Blood Distribution of Antiplasmodial Aminopeptidase-1 Inhibitors

Rebecca Deprez-Poulain,*[,†,‡,§] Marion Flipo,[†,‡,§] Catherine Piveteau,[†,‡,§] Florence Leroux,[†,‡,§] Sandrine Dassonneville,[†,‡,§] Isabelle Florent,[∥] Louis Maes,[⊥] Paul Cos,[⊥] and Benoit Deprez*[,†,‡,§]

[†]INSERM U761, Biostructures and Drug Discovery and Faculté de Pharmacie, Université Lille Nord de France, 3 rue du Pr Laguesse, Lille F-59000, France

[‡]Institut Pasteur de Lille, IFR 142, Lille F-59021, France

[§]PRIM, Lille F-59000, France

[∥]CNRS/MNHN, UMR7245, Molécules de Communication et Adaptation des Micro-organismes, Adaptation des Protozoaires à leur Environnent, F-75231 Paris, France

[⊥]Laboratory of Microbiology, Parasitology & Hygiene, Faculty of Pharmaceutical, Biomedical and Veterinary Sciences, University of Antwerp, B-2020 Antwerp, Belgium

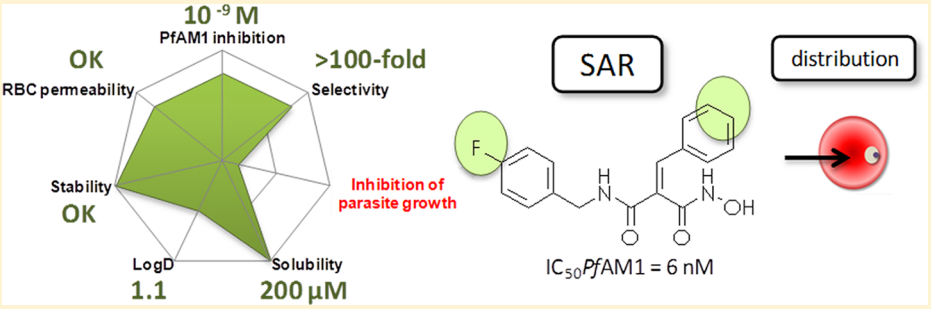

ABSTRACT: Malaria is a severe infectious disease that causes between 655 000 and 1.2 million deaths annually. To overcome the resistance to current drugs, new biological targets are needed for drug development. Aminopeptidase M1 (*Pf*AM1), a zinc metalloprotease, has been proposed as a new drug target to fight malaria. Herein, we disclosed the structure–activity relationships of a selective family of hydroxamate *Pf*AM1 inhibitors based on the malonic template. In particular, we performed a "fluoro-scanning" around hit **1** that enlightened the key positions of the halogen for activity. The docking of the best inhibitor **2** is consistent with in vitro results. The stability of **2** was evaluated in microsomes, in plasma, and toward glutathione. The in vivo distribution study performed with the nanomolar hydroxamate inhibitor **2** (BDM14471) revealed that it reaches its site of action. However, it fails to kill the parasite at concentrations relevant to the enzymatic inhibitory potency, suggesting that killing the parasite remains a challenge for potent and druglike catalytic-site binding *Pf*AM1 inhibitors. In all, this study provides important insights for the design of inhibitors of *Pf*AM1 and the validity of this target.

INTRODUCTION

The WHO/TDR initiative promotes drug target validation for neglected diseases.[1] As such, innovative strategies are being developed to discover new antiplasmodial targets and may include a target-driven approach by cell-based screening,[2] drug repositioning, and chemogenomics.[3,4] In this context, the *Plasmodium* proteases are putative targets.[5−8] Their study benefits from the successful work done on proteases in other pathologies, such as AIDS, hypertension, and type-II diabetes.[9,10] Among the metalloproteases of *Plasmodium*, falcilysin is involved in the intravacuolar digestion of globin and has no reported inhibitor.[11] On the other hand, aminopeptidases degrading oligopeptides resulting from hemoglobin digestion are well-studied.[12−14] Recently, inhibitors of LAP (leucine-aminopeptidase), a hexameric aminopeptidase of the M17-family, have been described.[15,16]

Florent et al. characterized the aminopeptidase M1 (*Pf*AM1 or *Pf*M1AAP) that shows a strict aminopeptidase activity at pH 7.4 and a broad substrate spectrum.[17,18] *Pf*AM1 localizes differently in trophozoites and schizonts, suggesting a particular role in the intraerythrocytic life of the parasite. *Pf*AM1 degrades oligopeptides resulting from hemoglobin digestion either in the vacuole[19] or the cytosol.[20] The inhibition of *Pf*AM1 by bestatin analogues induces swollen digestive vacuoles due to the accumulation of oligopeptides.[21] Also, a role in the reinvasion of erythrocytes has been found, in agreement with the observation of Kitjaroenthan et al.[22] Studies on *Pf*AM1 localization suggest that it is trafficked via the parasitophorous

Received: July 12, 2012
Published: November 23, 2012

dx.doi.org/10.1021/jm301506h | *J. Med. Chem.* 2012, 55, 10909−10917

vacuole.[23] *Pf*AM1 is also present in the nucleus, but so far no function can be related to its nuclear localization.[19]

Given these results, *Pf*AM1 can be considered an attractive candidate to initiate screening and lead optimization. Our research group was the first to describe *Pf*AM1 screening and the first two series of hydroxamic nonpeptidic nonselective *Pf*AM1 inhibitors with a mixed mode of action.[24] The screening of a focused library of zinc-binding molecules[25] resulted in a malono-hydroxamic druggable hit, **1**.[26] Chemical modifications explored the introduction of steric constrains at the malonic position and led to the discovery of **2**, a nanomolar selective inhibitor of *Pf*AM1. **2** shows good physicochemical, in vitro plasma stability and promising antiplasmodial activity in vitro.[26] Other inhibitors, such as phosphonopeptides, were subsequently published[27,28] and were designed as mixed inhibitors of the aminopeptidases of the M1 and M17 families. The binding of one nonselective compound to *Pf*AM1 was assessed by cocrystallization with the recombinant enzyme whose X-ray structure had been published.[29] Recently, peptide-based bestatin analogues were also disclosed.[28]

This paper reports the further optimization of our inhibitors whereby initial medicinal chemistry experiments revealed that the introduction of a fluorine on the scaffold had a significant impact on the inhibitory activity.[26] First, the effect on potency of systematic moving of fluorine ("fluorine scanning")[30,31] around compounds **1** and **2** was evaluated. Also substitution at the malonic carbon and the introduction of a pyridine to introduce a positive charge, which is a hallmark of many antiplasmodials, were explored. Analogues on *Pf*AM1 covering a 2.5 log range of IC_{50}s were tested in vitro on the intraerythrocytic cycle. We analyze these results in the light of structure–activity relationships on the isolated enzyme and distribution/stability data of the most active *Pf*AM1 inhibitor.

RESULTS AND DISCUSSION

Synthesis of Inhibitors 1–14. Inhibitors were synthesized as described in Schemes 1 and 2. Precursors **5a,b,d,e**, **1–4**, and **12** were synthesized as previously described.[26,32] **5c** was synthesized by a Knoevenagel reaction between 4-fluorobenzaldehyde and ethyl *N-tert*-butoxymalonamate in refluxed ethanol in the presence of piperidine. The resulting ester was saponified to give carboxylic acid **5c** as a single *E*-isomer as determined by ROESY NMR.

5a–d reacted with the corresponding amine after activation of the carboxylic acid function using either ethylchloroformate or EDCI/HOBt. The deprotection of the hydroxamate was performed in acidic conditions to give compounds **6-11**, **13**, and **14**.

Compound **12** was obtained from **5e** by coupling first the 4-fluorobenzylamine. Then, the ester was saponified, and the resulting carboxylic acid was activated and reacted with trityle-protected hydroxylamine. The final deprotection was performed in TFA/DCM.

***Pf*AM1 Inhibition and Selectivity toward *p*APN.** In these series, hit **1** (IC_{50} = 27 nM) and its analogue **2** (IC_{50} = 6 nM) bearing a *p*-fluorobenzene ring were more active than **4** (IC_{50} = 125 nM) deprived of a halogen (Table 1).[26] Fluorine is often used in medicinal chemistry[33–35] as it is sterically small and most often chemically inert. It is the most electronegative halogen and forms stable bonds with carbon that are poorly polarizable. Compounds **6–8**, resulting from "fluorine scanning", display a 10-fold decrease in potency. This illustrates the importance of the presence of fluorine in the para-position of

Scheme 1. Synthesis of Carboxylic Acid Precursors 5a–e[a]

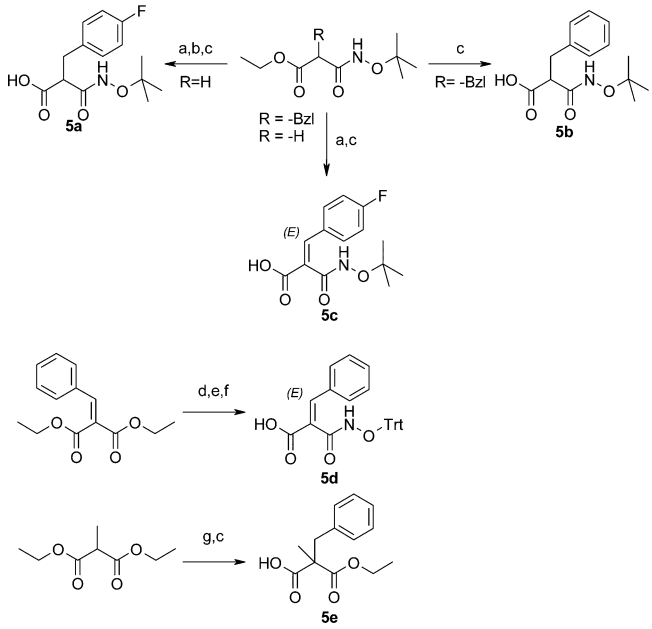

[a](a) *p*-Fluorobenzaldehyde, piperidine, abs EtOH, reflux, 3.5 h; (b) $NaBH_3CN$, CH_3CN, 24 h, rt; (c) KOH, abs EtOH, overnight, rt; (d) 1 equiv LiOH, THF, H_2O, 4 h, rt; (e) (i) 1.2 equiv oxalyl chloride, DCM, cat. DMF, 45 min, 0 °C, (ii) 3 equiv DIEA, 0.85 equiv *O*-tritylhydroxylamine, DCM, 0 °C then rt, 3 h; (f) 4 equiv LiOH, THF, H_2O, overnight, rt; (g) (i) EtONa, EtOH, 1 h, 50 °C, (ii) benzyl bromide, 2 h, 50 °C.

Scheme 2. Synthesis of *Pf*AM1 inhibitors 6–14[a]

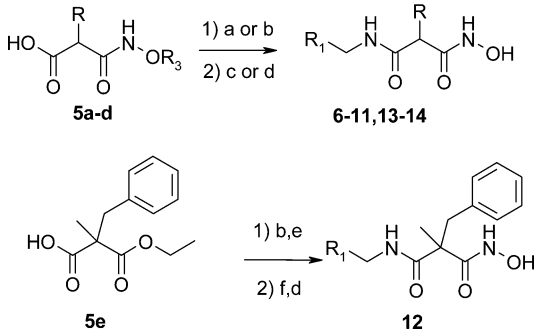

[a](a) (i) 1.1 equiv ethylchloroformate, 1.1 equiv TEA, DCM, 30 min, 0 °C, (ii) 1.1 equiv R_1–CH_2NH_2, 1 h, rt; (b) R_1–CH_2NH_2, EDCI/HOBt, DMF/DIEA, 5 h, rt; (c) BTFA (0.75 M/TFA; 25 equiv) with 0.4% H_2O, rt for t-Bu; (d) TFA 2%/DCM, TIS, 10 min, rt for trityl; (e) KOH, abs EtOH, overnight, rt; (f) (i) 1.1 equiv ethyl chloroformate, 1.1 equiv TEA, DCM, 30 min, 0 °C, (ii) 1.1 equiv H_2N-OTrt, HCl, 1 h, rt.

the benzylamido moiety rather than in ortho- or meta- position or on the other phenyl ring. Interestingly, compound **9**, which has a fluorine atom at this critical position and an additional fluorine, is less active than compound **1**. This finding suggests that fluorine on the benzyl malonyl moiety is exposed to a fluorophobic region. The same trend is observed for unsaturated compounds **10** and **11**, analogues of **2** (IC_{50} = 6 nM), which are 7–10-fold less potent. Nevertheless, the beneficial unsaturation compensates for bad fluorine position.

Substitution of a hydrogen atom by a methyl group on the malonic carbon of **1** (compound **12**) induced a 2-fold loss in

dx.doi.org/10.1021/jm301506h | J. Med. Chem. 2012, 55, 10909–10917

Table 1. Inhibition of *Pf*AM1, *p*APN by Compounds 1−3 and 5−13

Compound	Structure	*Pf*AM1 inhibition IC_{50} (nM)[a,c]	*p*APN inhibition IC_{50} (nM)[b,c]
1	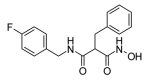	27	3616
2(BDM14471)	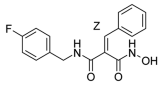	6	1372
3	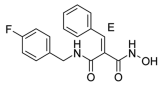	330	>10000
4	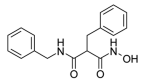	125	>10000
6	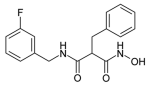	210	2333
7	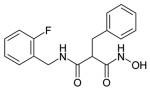	256	2223
8	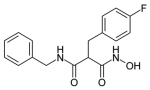	310	1324
9	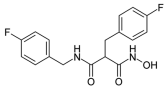	258	3956
10	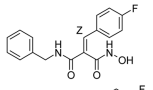	69	2400
11	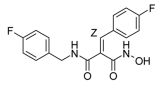	43	4200
12	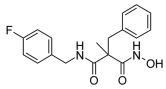	56	>10000
13	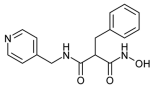	1050	4550
14	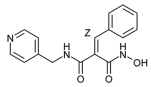	440	2000

[a]IC_{50} of bestatine (nM) was 284. [b]IC_{50} of bestatine (nM) was 2700. [c]Mean of three experiments; standard error was below 10%.

activity, while the substitution of *p*-fluorophenyl by a pyridine ring[36] in compounds **1** and **2** enabled the exploration of the properties of the enzyme pocket and generated a positive charge. Compounds **13** and **14** were about 50 times less active than their analogue.

All compounds were shown to be selective for the parasitic enzyme versus the mammalian enzyme APN (neutral aminopeptidase). The highest selectivity ratios were observed for compounds **2** and **11**.

To rationalize structure−activity relationships, compound **2** was docked in *Pf*AM1 (using PDB ID 3T8V) (Figure 1). The hydroxamate moiety binds the Zn^{2+} ion and is involved in a hydrogen bond with Glu497. The S1 pocket of the enzyme is hydrophobic and able to undergo major conformational changes upon ligand binding.[28] It is characterized by hydrophobic residues (Gln317, Val459, Met462, Glu572, Tyr575, Met1034)[29] that can accommodate the benzylmalonyl substituent of **2** or larger substituents.[26] The introduction of a fluorine atom at this position, although tolerated, is not critical for activity (compound **1** vs **8** and **9**, Table 1). Interestingly, a T-staking[37,38] between Tyr575 and phenylmeth-(*Z*)-ylidene moeity is observed (Figure 1), explaining why the *Z*-isomer (**2**) is more active than the *E*-isomer (**3**).

The amide function is engaged in two hydrogen bonds with Gly460 and Ala461 backbones. The S′1 pocket is also delimited with hydrophobic residues (Thr492, Val493, and Val523).[29] Although a cation−π interaction is observed between the benzyl group of **2** and Arg489, the introduction of the electron-withdrawing fluorine has a positive impact on activity (**2** vs **4**, Table 1). This may be the result of an increased desolvation entropy upon binding in this pocket. Also, the presence of the positively charged Arg489 explains why pyridine is less tolerated on that position (compounds **13**, **14**, Table 1).

Parasite Growth Inhibition and Cytotoxicity. None of the compounds tested was cytotoxic for MRC5 cells (IC_{50} > 32 μM, Table 2). Compounds **1**, **2**, **6**−**9**, **11**, and **12** inhibited

Table 2. Inhibition of Parasite Growth by Compounds 1, 2, 6−9, 11−13, and 15

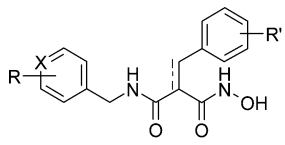

1,2,6-9,11-13

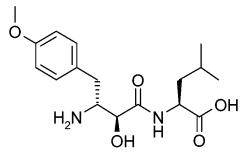

15

compound	*Pf*AM1[a] inhibn IC_{50} (nM)	parasite growth[b] IC_{50} (μM)	cytotoxicity IC_{50} (μM)
1	27	17.4 (59[f])	>64.0
2	6	11.0 (24[f])	32.0
6	210	24.7	>64.0
7	256	37.9	>64.0
8	310	36.5	>64.0
9	258	41.6	>64.0
11	43	30.4	32.2
12	56	50.1	>64.0
13	1050	>64.0	>64.0
bestatine[d]	478[e]	8−21[g]	_[c]
hPheP[CH_2]Phe[d]	79[e]	24−62[g]	_[c]
15[d]	43[e]	6.4[g]	_[c]

[a]Inative enzyme. [b]Mean of at least three experiments; K1 strain, IC_{50} of chloroquine (nM) was 154. [c]Not determined. [d]Reference 28 or 29. [e]Recombinant enzyme. [f]FcB1 strain, IC_{50} of chloroquine (nM) was 110. [g]3D7 strain, IC_{50} of chloroquine (nM) was 10.

parasite growth at IC_{50} values ranging between 11 and 50 μM (Table 2), which is comparable to other *Pf*AM1-selective or mixed *Pf*AM1/LAP inhibitors[12,16,27,29] or bestatine analogues.[28] However, there is a lack of correlation between enzymatic and parasite activities. Compounds very similar in structure, yet displaying low nanomolar to micromolar potencies on the enzymatic assay, show poor activity on the parasite (i.e., **6** vs **1**; **10** vs **8**).

To elucidate this large activity gap and the lack of correlation between the in vitro inhibition of *Pf*AM1 and the parasite growth inhibition, in vitro ADME parameters were explored for a set of analogues to select a compound for in vivo pharmacokinetics.

in Vitro ADME Parameters for 2. Some key physicochemical parameters were measured for the most potent and

dx.doi.org/10.1021/jm301506h | J. Med. Chem. 2012, 55, 10909−10917

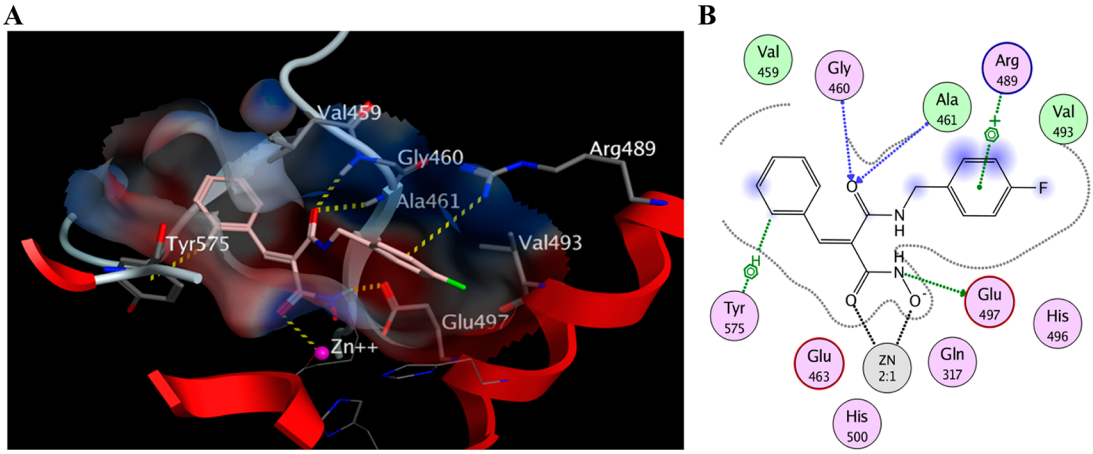

Figure 1. Binding of **2** in *Pf*AM1. (A) Docking of **2** in the enzyme (PDB ID: 3T8V). Zinc ion is colored magenta. The atoms oxygen and nitrogen are colored red and blue, respectively, fluorine is colored green, and carbon is shown in light pink or light gray for, respectively, **2** or key residues of *Pf*AM1. Specific hydrogens are colored white. (B) Schematic representation of the interactions of **2** with *Pf*AM1, featuring the three-letter codes of amino acids lining the binding pocket. Polar residues are pink (blue circles for positively charged, red circles for negatively charged), and apolar residues are green. Metal contacts are represented as black dotted lines. Hydrogen bonds in blue (acceptor) or green (donor) arrows, respectively. Arene-H and arene-positive charge are represented as green dotted lines.

selective compounds **1**, **2**, and **11** (Table 3). Compounds **1** and **2** have comparable solubilities and log *D*, while **11** is slightly more hydrophobic and less soluble. All three compounds are stable in human plasma, but compound **2** is by far the most stable compound in rodent plasma, which is critical for in vivo pharmacokinetics. These stabilities are coherent with previous data on hydroxamate stabilities.[32]

Table 3. Solubility, log *D*, and Plasma Stabilities for 1, 2, and 11

			plasma stability (h)[b]	
compd	solubility (μM)[a]	log *D* (pH 7.4)[a]	rat	human
1	>200	1.2	0.8	>24
2	198	1.1	22	>24
11	190	1.7	3.0	>24

[a]Solubility and log *D* are measured from a DMSO stock solution. [b]Half-life plasma stability at 37 °C using LC−MS/MS (MRM detection mode).

Before the pharmacokinetic evaluation in mice, **2** was further characterized in vitro. **2** displays a Michael acceptor function that may be sensitive to soft nucleophiles like thiols. An in vitro glutathione alkylation study[39] revealed that compound **2** is isomerized in vitro in its *E*-isomer **3** through the GSH-adducts production (*Z*/*E* 54/46, after 24 h). The proportion of combined GSH-adducts of the two unsaturated isomers reaches 50% at 24 h. **2** was also tested in vitro for mouse microsomal stability and was found to be very stable in a classic 30-min assay. Interestingly, this stability was observed for both the oxidative and the nonoxidative metabolism, suggesting that no hydrolysis of the hydroxamate moiety occurs through esterase activity.

Pharmacokinetics of 2 in Mice. Female CD1 mice received **2** at 50 mg/kg intraperitoneally to evaluate whether it would be concentrated enough for in vivo activity against *Plasmodium berghei* infection. As the parasite is located in erythrocytes, both the plasma concentration and the distribution in erythrocytes were investigated. **2** was formulated in 50/50 DMSO/PBS at 10 mg/mL. Blood was collected at regular time intervals after dosing (Figure 2). Plasma and red blood cells (RBCs) were fractionated, and quantification of **2** was performed using LC−MS/MS.

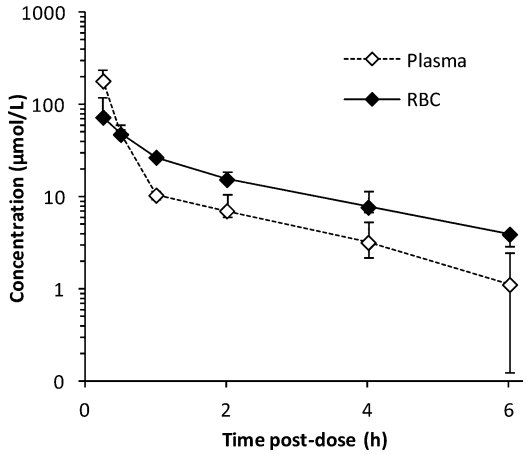

Figure 2. Concentration−time profile for compound **2**. Concentrations in plasma (◇) or red blood cells (◆) found in female CD1 mice receiving single ip administration at 50 mg/kg. Symbols represent averages from two mice. Plasma and red blood cell data are presented as μmol/L.

Following a single dose, **2** could be measured readily after dosing and until the end of the experiment (6 h postdose) (Figure 2), showing a plasma elimination half-life of 1 h (from 1 to 6 h; Table 4). As expected from the stability studies, only traces of carboxylic acid were formed, indicating that the hydroxamate was not a primary site of metabolism. Fortunately, as opposed to in vitro results, no GSH-mediated isomerization

Table 4. Pharmacokinetic Parameters of 2 in Female Mice

matrix	dose (mg/kg ip)	T_{last} (h)	$AUC_{0\rightarrow last}$ (μmol h/L)	$AUC_{0\rightarrow\infty}$ (μmol h/L)	$T_{1/2}$ (h)
plasma	1 × 50	6	66	68	1.0
RBCs			90	98	1.5

dx.doi.org/10.1021/jm301506h | *J. Med. Chem.* 2012, 55, 10909−10917

occurred in mice as *E*-isomer **3** was not detected in the in vivo experiment either in plasma or in red blood cells. **2** penetrates red blood cells with a significant $AUC_{0\rightarrow\infty}$ of 98 μmol h/L measured in red cells (Figure 2, Table 4).

The global AUC for **2** in red blood cells is even higher than that in plasma, suggesting that **2** enters and accumulates in RBCs. Thus, the gap between in vitro and in vivo activity could not be explained by a lack of host cell penetration. However, it could possibly be explained by the trapping of the compound by a component of red blood cells before it is able to reach the parasite. It is known that Zn^{2+} ion ligands, such as dorzolamide, can be trapped in RBC by carbonic anhydrase.[40] Carbonic anhydrase is a zinc metallohydrolase that is located in red blood cells in high concentrations (150 μM total isoforms). Nevertheless, **2** does not inhibit *h*CAII (0% inhibition at 10 and 50 μM, tested in duplicate), indicating that it does not bind carbonic anhydrase and likely is free to enter the parasitic cell from the cytoplasm of red blood cells. In all, this shows that the gap between enzymatic inhibitory potency and antiplasmodial activity cannot be explained by any of the molecular properties of **2** tested by us.

CONCLUSION

On the basis of literature data, *Pf*AM1 has been regarded as essential to the malaria parasite. However, none of its described inhibitors, including ours, was able to kill the parasite at concentrations below 1 μM, raising the question of the pharmacological relevance of inhibiting *Pf*AM1 to treat malaria. To formulate a conclusion, we must take into account that the pharmacological activity of an inhibitor is not only determined by its binding to the target and its inhibitory potency, but also by its ability to reach the target at a sufficient concentration for a sufficient period of time. The lack of pharmacokinetic data on inhibitors reported earlier made it difficult to interpret their poor antiplasmodial potency. In this paper, we report the first structurally homogeneous family of inhibitors demonstrating a 100-fold range of enzyme potency, together with antiplasmodial activities and key pharmacokinetic parameters.

Structure−activity relationships established by "fluorine scanning" showed that the best position for fluorine is para on the benzylamido group. Substitution at the malonic carbon is tolerated, whereas introduction of a pyridine is deleterious for activity. The range of compounds tested here spanned a 2.5 log scale of inhibitory potency on the isolated enzyme. However, in this population, we were not able to observe any correlation between enzymatic potency and antimalarial activity. To rule out potential compound-related issues in the course of the validation of *Pf*AM1 as a drug target, we performed stability and distribution studies with **2** (BDM14471), our most promising inhibitor, taking into account potency, physicochemical parameters, and metabolic stability. Pharmacokinetic experiments in mice evidenced a significant distribution of **2** in plasma and red blood cells until 6 h after dosing. In this experiment, **2** reached micromolar concentrations within the red blood cells that harbor the parasites in culture. Altogether, these results show that the compound reaches the site of action but fails to kill the parasite at concentrations relevant to the enzymatic inhibitory potency, suggesting that killing the parasite remains a challenge for potent and druglike catalytic site binding *Pf*AM1 inhibitors. A working hypothesis to explain these results could be that the catalytic activity of the *Pf*AM1 is not critical for the survival of the parasite at the intraerythrocyte stage. In this situation, other nonproteolytic regulatory functions of *Pf*AM1 may have to be targeted to produce antimalarial drug candidates.

MATERIALS AND METHODS

General Chemistry. ^{1}H and ^{13}C NMR were recorded at room temperature on a Bruker DPX 300 at 300 and 75 MHz, respectively. Chemical shifts are in parts per million (ppm). The assignments were made using one-dimensional (1D) ^{1}H and ^{13}C spectra or two-dimensional (2D) HSQC and COSY spectra. Mass spectra were recorded on a LC−MS system (Waters). HPLC analysis were performed using a C_{18} TSK-GEL Super ODS 2 μm particle size column, dimensions 50 × 4.6 mm. A LC−MS gradient starting from 100% H_2O/0.1% formic acid and reaching 20% H_2O/80% MeOH/0.08% formic acid within 5 min at a flow rate of 1 mL/min was used. purity (%) was determined by reversed-phase chromatography HPLC using UV detection (215 nm), and all compounds showed purities greater than 95%. All commercial reagents and solvents were used without further purification.

Coupling Reactions for Amide Bond formation. (a) Carboxylic acid (0.66 mmol, 1 equiv) was dissolved in DCM (7 mL), and TEA (102 μL, 0.73 mmol, 1.1 equiv) was added. The mixture was cooled at 0 °C (ice bath) and ethylchloroformate (70 μL, 0.73 mmol, 1.1 equiv) was added dropwise. The reaction mixture was stirred 30 min at 0 °C and then the desired amine (0.73 mmol, 1.1 equiv) was added. The organic layer was stirred for 1 h at room temperature and then evaporated. The crude product was dissolved in ethyl acetate; washed twice with aq $NaHCO_3$ 5%. once with water, and once with aq NaCl; dried over $MgSO_4$; filtered; and evaporated. The product was purified by thick-layer chromatography (DCM 100%) and/or precipitated in petroleum ether (40−60) to give the expected amide. Alternatively, (b) carboxylic acid (0.1M/DMF, 1 equiv), DIEA (2.4 equiv), EDCI (1.1 equiv), and HOBt (1.1 equiv) were stirred for 5 min at room temperature. Then the appropriate amine (0.1 M/DMF, 1 equiv) and DIEA (2 equiv) were added. The mixture was stirred for 5 h at room temperature, and then solvents were removed under reduced pressure. The residue was dissolved in AcOEt and the organic phase was washed with aqueous $NaHCO_3$ 5% (six times) and NaCl (once). The organic layer was dried over $MgSO_4$ and evaporated under reduced pressure. The residue was precipitated in petroleum ether.

***tert*-Butyl Deprotection.** *tert*-Butylated intermediate was dissolved in a suspension of BTFA (0.75 M/TFA, 25 equiv) with 0.4% H_2O. The reaction mixture was stirred for 4−5.5 h at room temperature. Solvents were removed under reduced pressure and the residue was dissolved in water. The aqueous phase was basified with 1 M NaOH to pH 7 and extracted three times with AcOEt. The organics layers were dried over $MgSO_4$, filtered, and evaporated. The residue was precipitated in ether−pentane. Yields given are those of the deprotection step.

Trityl Deprotection. Tritylated intermediate was dissolved in TFA 2%/DCM, and triisopropylsilane was added drop-by-drop until the yellow color disappeared. The reaction mixture was stirred for 5 min at room temperature, solvents were removed under reduced pressure, and the residue was washed with ether−pentane. Yields given are those of the deprotection step.

(*E*)-2-*tert*-Butoxycarbamoyl-3-(4-fluorophenyl)acrylic Acid (5c). 4-Fluorobenzaldehyde (32.0 mmol, 1 equiv) was added to a solution of ethyl N-*tert*-butoxymalonate (7.163 g, 35.2 mmol, 1.1 equiv) and piperidine (1 mL) in abs ethanol (150 mL). The solution was refluxed for 3.5 h and solvent was removed under reduced pressure. The crude product was purified by flash chromatography (DCM/MeOH 98/2) to give ethyl (*Z*/*E*)-2-*tert*-butoxycarbamoyl-3-(4-fluorophenyl)acrylate in 71% yield (85% purity). ^{1}H NMR ($CDCl_3$) δ ppm: 1.21−1.29 (m, 12H), 4.24 (q, *J* = 7.1 Hz, 2H), 7.01 (t, *J* = 8.6 Hz, 2H), 7.51−7.55 (m, 2H), 7.69 (s, 1H), 7.86 (s, NH). MS: $(MH)^+$ *m*/*z* 310. MS: $(MNa)^+$ *m*/*z* 332. The later ethyl ester (3.478 g, 11.25 mmol) is dissolved in abs ethanol (115 mL), and KOH (2.57 g, 45 mmol, 4 equiv) is added. The mixture is stirred overnight at room temperature and then evaporated. The crude

dx.doi.org/10.1021/jm301506h | J. Med. Chem. 2012, 55, 10909−10917

product is dissolved in water. The aqueous phase is acidified with 1 N aq HCl until pH 1 and then the carboxylic acid is extracted with ethyl acetate (4 × 20 mL). The organic layers are pooled, dried over $MgSO_4$ and evaporated to give **5c** as a yellow powder in 92% yield (95% purity). ^{1}H NMR (DMSO-d_6) δ ppm: 1.17 (s, 9H), 7.28 (t, J = 8.9 Hz, 2H), 7.61 (s, 1H), 7.64−7.69 (m, 2H), 10.83 (s, NH), 12.85 (s, OH). tr_{LC-MS}: 4.19 min. MS: $(MH)^+$ m/z 282. Mp: 188−190 °C.

2-Benzyl-*N*-(4-fluorobenzyl)-*N*′-hydroxymalonamide (1). White powder, yield 88% (100% purity). ^{1}H NMR (DMSO-d_6) δ ppm: 2.96−3.10 (m, 2H), 3.35−3.40 (m, 1H), 4.16 (dd, J = 15, J = 5.7 Hz, 1H), 4.27 (dd, J = 15, J = 6 Hz, 1H), 7.04−7.27 (m, 9H), 8.40 (t, J = 5.6 Hz, NHCO), 8.93 (s, OH), 10.58 (s, CONHO). ^{13}C NMR (DMSO-d_6) δ ppm: 35.0, 42.1, 52.5, 115.5 (d, J_{CF} = 21.1 Hz), 126.8, 128.8, 129.4, 129.5 (d, J_{CF} = 8.4 Hz), 136.0 (d, J_{CF} = 2.3 Hz), 139.6, 161.7 (d, J_{CF} = 240.4 Hz), 166.3, 168.9. tr_{LC-MS}: 4.31 min. MS: $(MH)^+$ m/z 317. Mp: 193−194 °C.

***N*-(4-Fluorobenzyl)-*N*′-hydroxy-2-[1-phenylmeth-(*Z*)-ylidene]malonamide (2).** White powder, yield 37% (overall) (99% purity). ^{1}H NMR (DMSO-d_6) δ ppm: 4.37 (d, J = 6.0 Hz, 2H), 7.12−7.18 (m, 2H), 7.32−7.40 (m, 5H), 7.43 (s, 1H), 7.51−7.54 (m, 2H), 8.26 (t, J = 6.0 Hz, NHCO), 9.13 (s, OH), 11.01 (s, CONHO). ^{13}C NMR (DMSO-d_6) δ ppm: 42.6, 115.6 (d, J_{CF} = 21 Hz), 129.3, 129.5, 129.9, 130.1, 130.6, 134.2, 136.2, 137.3, 161.8 (d, J_{CF} = 246 Hz), 163.5, 164.6. tr_{LC-MS}: 4.23 min. MS: $(MH)^+$ m/z 315.

***N*-(4-Fluorobenzyl)-*N*′-hydroxy-2-[1-phenylmeth-(*E*)-ylidene]malonamide (3).** White powder, yield 50% (overall) (99% purity). ^{1}H NMR (DMSO-d_6) δ ppm: 4.30 (d, J = 6.0 Hz, 2H), 7.08−7.37 (m, 10H), 8.86 (t, J = 6.0 Hz, NHCO), 9.08 (br s, OH), 10.70 (br s, CONHO). ^{13}C NMR (DMSO-d_6) δ ppm: 42.3, 115.3 (d, J_{CF} = 20 Hz), 128.9, 129.5, 129.6, 129.8, 130.3 (d, J_{CF} = 12 Hz), 132.0, 134.3, 135.2, 161.4 (d, J_{CF} = 225 Hz), 163.3, 166.2. tr_{LC-MS}: 4.41 min. MS: $(MH)^+$ m/z 315.

2,*N*-Dibenzyl-*N*′-hydroxymalonamide (4). White powder, yield 84% (100% purity). ^{1}H NMR (DMSO-d_6) δ 3.00−3.08 (m, 2H), 3.30 (t, J = 6.75 Hz, 1H), 4.20 (dd, J = 5.1 Hz, J = 15 Hz, 1H), 4.30 (dd, J = 5.4 Hz, J = 15 Hz, 1H), 7.10−7.23 (m, 10H), 8.20−8.23 (m, NHCO), 10.44 (s, CONHO). ^{13}C NMR (DMSO-d_6) δ 35.1, 42.7, 52.7, 126.6, 127.1, 127.5, 128.6, 128.7, 129.3, 139.4, 139.6, 166.2, 168.6. tr_{LC-MS}: 4.25 min. MS: $(MH)^+$ m/z 299. Mp: 167−169 °C.

2-Benzyl-*N*-(3-fluorobenzyl)-*N*′-hydroxymalonamide (6). White powder, yield 90% (100% purity). ^{1}H NMR (DMSO-d_6) δ ppm: 2.98−3.12 (m, 2H), 3.29−3.35 (m, 1H), 4.21 (dd, J = 15.6 Hz, J = 6.0 Hz, 1H), 4.30 (dd, J = 15.6 Hz, J = 6.3 Hz, 1H), 6.93−7.06 (m, 3H), 7.18−7.33 (m, 6H), 8.31 (t, J = 6.0 Hz, NH), 8.95 (s, OH), 10.49 (s, CONHO). tr_{LC-MS}: 4.51 min. MS: $(MH)^+$ m/z 317. Mp: 167.5−168.8 °C.

2-Benzyl-*N*-(2-fluorobenzyl)-*N*′-hydroxymalonamide (7). White powder, yield 70% (100% purity). ^{1}H NMR (DMSO-d_6) δ ppm: 3.03−3.07 (m, 2H), 3.30−3.35 (m, 1H), 4.23 (dd, J = 15.6 Hz, J = 5.6 Hz, 1H), 4.32 (dd, J = 15.6 Hz, J = 6.0 Hz, 1H), 7.02−7.32 (m, 9H), 8.25 (t, J = 5.7 Hz, NH), 8.95 (s, OH), 10.47 (s, CONHO). tr_{LC-MS}: 4.20 min. MS: $(MH)^+$ m/z 317. Mp: 182.3−184.7 °C.

***N*-Benzyl-2-(4-fluorobenzyl)-*N*′-hydroxymalonamide (8).** White powder, yield 23% (95% purity). ^{1}H NMR (DMSO-d_6) δ ppm: 3.01−3.05 (m, 2H), 3.28 (t, J = 7.8 Hz, 1H), 4.18 (dd, J = 5.4 Hz, J = 15.3 Hz, 1H), 4.29 (dd, J = 6.0 Hz, J = 15.3 Hz, 1H), 7.04−7.11 (m, 4H), 7.19−7.29 (m, 5H), 8.24 (t, J = 6.0 Hz, NHCO), 8.95 (s, 1H, OH), 10.46 (s, CONHO). tr_{LC-MS}: 4.36 min. MS: $(MH)^+$ m/z 317.

2,*N*-Bis(4-fluorobenzyl)-*N*′-hydroxymalonamide (9). Beige powder, yield 21% (96% purity). ^{1}H NMR (DMSO-d_6) δ ppm: 3.00−3.04 (m, 2H), 3.26 (t, J = 7.8 Hz, 1H), 4.16 (dd, J = 5.7 Hz, J = 15.0 Hz, 1H), 4.26 (dd, J = 6.0 Hz, J = 15.0 Hz, 1H), 7.04−7.23 (m, 8H), 8.27 (t, J = 6.0 Hz, NHCO), 8.94 (s, 1H, OH), 10.47 (s, CONHO). tr_{LC-MS}: 4.50 min. MS: $(MH)^+$ m/z 335.

***N*-Benzyl-2-[1-(4-fluorophenyl)meth-(*Z*)-ylidene]-*N*′-hydroxymalonamide (10).** Beige powder, yield 15% (99% purity). ^{1}H NMR (DMSO-d_6) δ ppm: 4.39 (d, J = 5.4 Hz, 2H), 7.22−7.36 (m, 7H), 7.44 (s, 1H), 7.56−7.60 (m, 2H), 8.23 (t, J = 5.4 Hz, NHCO), 9.15 (s, OH), 11.03 (s, CONHO). tr_{LC-MS}: 4.17 min. MS: $(MH)^+$ m/z 315.

***N*-(4-Fluorobenzyl)-2-[1-(4-fluorophenyl)meth-(*Z*)-ylidene]-*N*′-hydroxymalonamide (11).** Beige powder, yield 15% (95% purity). ^{1}H NMR (DMSO-d_6) δ ppm: 4.36 (d, J = 5.7 Hz, 2H), 7.12−7.36 (m, 6H), 7.43 (s, 1H), 7.56−7.60 (m, 2H), 8.27 (t, J = 5.7 Hz, NHCO), 9.14 (s, OH), 11.03 (s, CONHO). tr_{LC-MS}: 4.36 min. MS: $(MH)^+$ m/z 333.

2-Benzyl-*N*-(4-fluorobenzyl)-*N*′-hydroxy-2-methylmalonamide (12). White powder, yield 60% (99% purity). ^{1}H NMR (CD_2Cl_2) δ ppm: 1.24 (s, 3H), 2.99 (s, 2H), 4.34 (s, 2H), 7.00−7.23 (m, 9H). tr_{LC-MS}: 4.66 min. MS: $(MH)^+$ m/z 331.

2-Benzyl-*N*-hydroxy-*N*′-pyridin-4-ylmethylmalonamide (13). White powder, yield 91% (99% purity). ^{1}H NMR (DMSO-d_6) δ ppm: 3.06−3.10 (m, 2H), 3.41 (t, J = 7.7 Hz, 1H), 4.47 (d, J = 5.7 Hz, 2H), 7.20−7.31 (m, 5H), 7.62 (d, J = 6.0 Hz, 2H), 8.63 (t, J = 5.7 Hz, CONH), 8.76 (d, J = 6.0 Hz, 2H), 10.64 (s, CONHO). tr_{LC-MS}: 2.08 min. MS: $(MH)^+$ m/z 300.

2-Benzylidene-*N*-hydroxy-*N*′-pyridin-4-ylmethylmalonamide (14). White powder, yield 90% (98% purity). ^{1}H NMR (DMSO-d_6) δ ppm: 4.58 (d, J = 5.7 Hz, 2H), 7.10−7.56 (m, 7H), 7.76 (s, 1H), 8.45−8.78 (m, 2H + NHCO), 11.09 (s, CONHO). tr_{LC-MS}: 2.14 min. MS: $(MH)^+$ m/z 298.

***Pf*AM1 Inhibition.** Native *Pf*AM1 was purified according to the procedure described by Allary et al.[17] and diluted 10 times in Tris−HCl buffer (25 mM, pH 7.4) before use. The assays were set up in 96-well plates. The compounds were tested at the concentration of 10 μM, and 33 μL of purified PfAM1 was preincubated for 10 min at room temperature with 33 μL of the inhibitor (30 μM in Tris−HCl buffer, 0.3% DMSO). Then 33 μL of the substrate Leu-pNA (K_m = 0.099 mM) (0.3 mM in Tris−HCl buffer) was added. The reaction kinetics performed at room temperature was followed on a UV-microplate reader MultiskanRC (Labsystems) at 405 nm. The control activity was determined by incubating the enzyme under the same conditions without inhibitor. Bestatin was used as the reference inhibitor (IC_{50} = 284 nM). The statistical Z' factor for the test was 0.82, allowing activities to be determined with a single point with a 95% confidence. Initial velocities are expressed in μmol min^{-1}. Data were normalized to the controls that represent V_{max}. For the determination of IC_{50}s, initial velocities were plotted as a function of inhibitor concentration, using XLfit software from IDBS.

***p*APN Inhibition.** Microsomal neutral aminopeptidase (APN) from porcine kidney was purchased from Sigma Inc. as an ammonium sulfate suspension [3.5 M $(NH_4)_2SO_4$ solution containing 10 mM $MgCl_2$, 10−40 units/mg protein]. The enzyme suspension was diluted 600-fold in Tris−HCl buffer (25 mM, pH 7.4) before use. The assays were performed in 96-well plates. The compounds were tested at the concentration of 10 μM, and 33 μL of purified APN was preincubated for 10 min at room temperature with 33 μL of the inhibitor (30 μM in Tris−HCl buffer, 0.3% DMSO). Then 33 μL of the substrate Leu-pNA (K_m = 0.099 mM) (0.3 mM in Tris−HCl buffer) was added. The reaction kinetics performed at room temperature was followed on a UV-microplate reader MultiskanRC (Labsystems, Finland) at 405 nm. The control activity was determined by incubating the enzyme in the same conditions without inhibitor. Bestatin was used as the reference inhibitor (IC_{50} = 2.7 μM). The statistical Z' factor for the test was 0.75, allowing activities to be determined with a single point with a 95% confidence.[39] Initial velocities are expressed in μmol min^{-1}. Data were normalized to the controls that represent V_{max}. For the determination of IC_{50}s, initial velocities were plotted as a function of inhibitor concentration, using XLfit software from IDBS.

In Vitro *Plasmodium falciparum* Culture and Drug Assay. Chloroquine-resistant *P. falciparum* 2/K 1-strain was cultured in human erythrocytes O^+ at 37 °C under a low oxygen atmosphere (3% O_2, 4% CO_2, and 93% N2) in RPMI-1640, supplemented with 10% human serum. Infected human red blood cells (200 μL, 1% parasitaemia, 2% hematocrit) were added to each well and incubated for 72 h. After incubation, test plates were frozen at −20 °C. Parasite multiplication was measured by the Malstat method. An amount of 100 μL of Malstat reagent was transferred to a new plate and mixed with 20 μL of the hemolysed parasite suspension for 15 min at room temperature. After addition of 20 μL of NBT/PES solution and 2 h of

incubation in the dark, the absorbance was spectrophotometrically read at 655 nm (Biorad 3550 UV microplate reader). Percentage growth inhibition was calculated compared to the negative blanks. IC_{50} values are calculated from the duplicate determinations with relative difference below 25%.

Cytotoxicity Test. MRC-5 SV2 cells, human fetal lung fibroblast, were cultivated in MEM supplemented with L-glutamine (20 mM), 16.5 mM sodium hydrogen carbonate, and 5% FCS at 37 °C and 5% CO_2. For the assay, 10^4 MRC-5 cells/well were seeded onto the test plates containing the prediluted compounds and incubated at 37 °C and 5% CO_2 for 72 h. After 72 h of incubation, parasite growth was assessed fluorimetrically by adding resazurin for 24 h at 37 °C. Fluorescence was measured using a GENios Tecan fluorimeter (excitation 530 nm, emission 590 nm). IC_{50} values are calculated from duplicate determinations with relative difference below 25%.

LC−MS/MS analysis. The LC−MS/MS system consisted of a Varian 1200L (Varian, Les Ulis, France) a Prostar 430 autosampler, a triple quadrupole mass spectrometer (Varian, Les Ulis, France) equipped with an electrospray ionization source, and a Prostar 325 detector. Analytes in incubation mixtures were separated by HPLC using a gelTSK C18 Super-ODS, 5 μm, 50 × 4.6 mm column (Interchim, Montluçon France). The mobile phase solvents used were (A) 0.01% formic acid in water and (B) 0.01% formic acid in acetonitrile. The following mobile phase gradient was applied: 0−100% B in 7.30 min, hold at 100% B for 1 min, 0−100% A in 0.30 min, and 100% A hold for 10 min. The injection volume was 10 μL and the flow rate of 1 mL/min. Approximately 30% of the eluent was introduced into the triple quadrupole mass spectrometer source. The source temperature of the mass spectrometer was maintained at 300 °C, the declustering potential was 50 V, and the curtain gas pressure was 1.5 mTorr. Collision energy and observed transitions were respectively individually optimized for each compound (MRM mode).

Docking. The docking of BDM14471 in *Pf*AM1 (using PDB structure 3T8V) was performed using MOE 2009.10 software from Chem Computing Group, Inc. Briefly, the protein was prepared within the MOE package using Gasteiger partial charges, and the generalized Born/volume integral formalism for protonation at pH 7. The protein atoms were kept as rigid and the ligands as flexible. No restraints were used during docking (conformational search using MM Iteration Limit 1000; all other standard parameters were set on default), but the binding modes were chosen on the basis of both the most favored predicted interaction energy with *Pf*AM1 and a proper chelating of the zinc ion by the hydroxamic function.

Solubility. A 40 μL portion of the 10 mM solution in DMSO of the sample was added to 1.960 mL of MeOH or PBS at pH 7.4. The samples were gently shaken for 24 h at room temperature, centrifuged for 5 min, and filtered over 0.45 μm filters. A 20 μL aliquot of each solution was added to 180 μL of MeOH and analyzed by LC−MS/MS. The solubility was determined by the ratio of mass signal areas PBS/MeOH.

log *D*. A 40 μL portion of the 10 mM solution in DMSO of the sample was added to 1.960 mL of a 1/1 octanol/PBS at pH 7.4 solution. The mixture was gently shaken 2 h at room temperature, and then the two phases were separated. A 20 μL aliquot of each solution was added to 180 μL of MeOH and analyzed by LC−MS/MS. log *D* was determined as the logarithm of the ratio of concentrations of product in octanol and PBS, determined by mass signals.

Plasma Stability. A 40 μL portion of the 5 mM solution in DMSO of the sample was added to 1.960 mL of rat plasma (male rat from Charles River Laboratories) to obtain a 100 μM final solution. The mixture was gently stirred for 96 h at 37 °C. Aliquots of 200 μL were taken at various times (from 0 to 96 h) and diluted with 200 μL of phosphoric acid (0.14 M), and 10 μL of the 2 mM solution in methanol of the internal standard was added. Compounds were extracted three times with 2 mL of AcOEt. The organic layer was evaporated, diluted with 200 μL of methanol, and quantified by LC−MS/MS, using a calibration curve.

Microsome Stability. All chemicals were obtained from Sigma-Aldrich (Steinheim, Germany). Solvents were from common sources and of HPLC grade. Stock solutions of all compounds were prepared in methanol at a concentration of 0.1 mM. Pooled male mouse (CD-1) liver microsomes were purchased from BD Gentest (Le Pont de Claix, France). All incubations were performed in duplicate in a shaking water bath at 37 °C. The incubation mixture was prepared in polypropylene tubes and contained 1 μM test compound (1% methanol), mouse liver microsomes (0.6 mg of microsomal protein/mL), 5 mM $MgCl_2$, 1 mM NADP, 5 mM glucose-6-phosphate, 0.4 U/mL glucose-6-phosphate dehydrogenase, and 50 mM potassium phosphate buffer (pH 7.4) in a final volume of 1.5 mL. Sampling points were taken at 5, 10, 15, 20, 25, 30, 45, and 60 min, and reactions were terminated by adding ice-cold acetonitrile containing 1 μM internal standard (1 vol). The samples were centrifuged for 10 min at 4000 g, 4 °C to pellet precipitated microsomal protein, and the supernatant was subjected to LC−MS/MS analysis. Control incubations were performed with denaturated microsomes with acetonitrile containing 1 μM internal standard, and sampling points were taken at 0 and 60 min (to evaluate the compound chemical stability under the experimental conditions). Quantitation of each compound was achieved by conversion of the corresponding analyte/internal standard peak area ratios in LC−MS/MS (MRM mode) to the percentage drug remaining, using the T_0 ratio values as 100%. In vitro intrinsic clearance (CL_{int} expressed as μL/min/mg) was calculated according to $CL_{int} = (\text{dose}/AUC_\infty)$, where dose is the initial amount of drug in the incubation mixture (1 μM) and AUC_∞ is the area under the concentration versus time curve extrapolated to infinity. The slope of the linear regression from log percentage remaining versus incubation time relationships ($-k$) was used in the conversion to in vitro $T_{1/2}$ values by in vitro $T_{1/2} = -0.693/k$.

GSH Sensitivity. In a 1 mL polypropylene tube are introduced 10 μL of a 10 μM solution of compound in acetonitrile with 145 μL of phosphate buffer (0.067 M at pH 7.4) and 145 μL of glutathione (5 mM/H_2O). The final compound concentration is 330 μM. After 1 h of room-temperature incubation, samples are analyzed by LC−MS to look for the glutathione conjugate.

***h*CA Inhibition.**[41] human erythrocyte carbonic anhydrase (*h*CA) activity was measured by following the reaction kinetics of hydrolysis of 4-nitrophenyl acetate (450 μM) on a UV-microplate reader at 400 nm, at CEREP, SA. The control activity was determined by incubating the enzyme under the same conditions without inhibitor. Acetazolamide (IC_{50} = 29 nM) was used as the reference inhibitor. The results are expressed as a percent inhibition of control specific activity (100 − (measured specific activity/control specific activity) × 100). This analysis was performed using a software developed at CEREP, SA.

Pharmacokinetic Study.[42] BDM14471 was formulated in 50/50 DMSO/PBS at 10 mg/mL and solubilized by short ultrasonic treatment (bath) if necessary. Twelve female CD-1 mice (approximately body weight 25−30 g) were given a single 50 mg/kg administration by intraperitonal injection and two mice served as negative control [no treatment (blank plasma)]. Food and drinking water remained available ad libitum throughout the trial. Blood samples (two mice per data point) were collected at 15 and 30 min and 1, 2, 4, and 6 h. The blood was collected intracardially at the stated time point using a heparinized syringe (1 droplet, 2% heparin) and transferred into an Eppendorf tube. The tubes were put on ice and centrifuged at 2600 rpm for 10 min to separate the plasma. The fractions of red cells or plasma were stored at 4 °C before analysis. Oasis-HLB 1 cm^3 (30 mg) flangeless cartridges from Waters Inc. were activated with 1 mL of methanol and then equilibrated with 1 mL of water Milli-Q. Samples were treated as follows. To 100 μL of plasma were added 2 μL of internal standard and 400 μL of water. To 100 μL of red blood cells was added 400 μL of water. The resulting suspension was sonicated and centrifuged, 400 μL of the supernatant was collected, and 2 μL of internal standard was added. The resulting mixtures (from plasma or red blood cells) were eluted on an HLB-column. The column was then washed with 0.25 mL of water/MeOH (95/5 v/v). The compounds were eluted with a solution of acetonitrile/water (95/5 v/v) containing 0.1% of formic acid. The eluate was evaporated and redissolved in 200 μL of methanol/mobile phase 60/40 (v/v) for LC−MS/MS analysis.

AUTHOR INFORMATION

Corresponding Author

*Phone: (+33) 320 964 947. Fax: (+33) 320 964 709. E-mail: rebecca.deprez@univ-lille2.fr (R.D-P.); benoit.deprez@univ-lille2.fr (B.D.).

Notes

The authors declare no competing financial interest.

ACKNOWLEDGMENTS

The authors thank Dr. N. Willand and B. Villemagne for their help with docking and visualization software. We are grateful to Inserm, Université de Lille2, and Institut Pasteur de Lille. This work was specifically funded by ≪Région Nord-Pas-de-Calais≫ and EC.

ABBREVIATIONS USED

AcOEt, ethyl acetate; AUC, area-under-curve; BTFA, boron tris(trifluoroacetate); APN, neutral aminopeptidase; CA, carbonic anhydrase; CH_3CN, acetonitrile; DCM, dichloromethane; DIEA, diisopropylethylamine; DMF, dimethylformamide; DMSO, dimethyl sulfoxide; EDCI, *N*-ethyl-3-(3-dimethylaminopropyl)carbodiimide; EtOH, ethanol; GSH, glutathione; HOBt, *N*-hydroxybenzotriazole; MeOH, methanol; PBS, phosphate-buffered saline; RBC, red blood cells; rt, room temperature; SAR, structure−activity relationship; TEA, triethylamine; TFA, trifluoroacetic acid; THF, tetrahydrofuran; TIS, triisopropylsilane; Trt, trityl.

REFERENCES

(1) Nwaka, S.; Ramirez, B.; Brun, R.; Maes, L.; Douglas, F.; Ridley, R. Advancing drug innovation for neglected diseases—Criteria for lead progression. *PLoS Negl. Trop. Dis* **2009**, *3*, e440.

(2) Crowther, G. J.; Napuli, A. J.; Gilligan, J. H.; Gagaring, K.; Borboa, R.; Francek, C.; Chen, Z.; Dagostino, E. F.; Stockmyer, J. B.; Wang, Y.; Rodenbough, P. P.; Castaneda, L. J.; Leibly, D. J.; Bhandari, J.; Gelb, M. H.; Brinker, A.; Engels, I. H.; Taylor, J.; Chatterjee, A. K.; Fantauzzi, P.; Glynne, R. J.; Van Voorhis, W. C.; Kuhen, K. L. Identification of inhibitors for putative malaria drug targets among novel antimalarial compounds. *Mol. Biochem. Parasitol.* **2011**, *175*, 21−29.

(3) Beghyn, T. B.; Charton, J.; Leroux, F.; Laconde, G.; Bourin, A.; Cos, P.; Maes, L.; Deprez, B. Drug to genome to drug: Discovery of new antiplasmodial compounds. *J. Med. Chem.* **2011**, *54*, 3222−3240.

(4) Beghyn, T. B.; Charton, J.; Leroux, F.; Henninot, A.; Reboule, I.; Cos, P.; Maes, L.; Deprez, B. Drug-to-genome-to-drug, step 2: Reversing selectivity in a series of antiplasmodial compounds. *J. Med. Chem.* **2012**, *55*, 1274−1286.

(5) Blackman, M. J. Proteases involved in erythrocyte invasion by the malaria parasite: Function and potential as chemotherapeutic targets. *Curr. Drug Targets* **2000**, *1*, 59−83.

(6) Blackman, M. J. Proteases in host cell invasion by the malaria parasite. *Cell. Microbiol.* **2004**, *6*, 893−903.

(7) Rosenthal, P. J. Hydrolysis of erythrocyte proteins by proteases of malaria parasites. *Curr. Opin. Hematol.* **2002**, *9*, 140−145.

(8) Wu, Y.; Wang, X.; Liu, X.; Wang, Y. Data-mining approaches reveal hidden families of proteases in the genome of malaria parasite. *Genome Res.* **2003**, *13*, 601−616.

(9) Drag, M.; Salvesen, G. S. Emerging principles in protease-based drug discovery. *Nat. Rev. Drug Discovery* **2010**, *9*, 690−701.

(10) Wegscheid-Gerlach, C.; Gerber, H.-D.; Diederich, W. E. Proteases of *Plasmodium falciparum* as potential drug targets and inhibitors thereof. *Curr. Top. Med. Chem.* **2010**, *10*, 346−367.

(11) Murata, C. E.; Goldberg, D. E. *Plasmodium falciparum* falcilysin: A metalloprotease with dual specificity. *J. Biol. Chem.* **2003**, *278*, 38022−38028.

(12) Skinner-Adams, T. S.; Stack, C. M.; Trenholme, K. R.; Brown, C. L.; Grembecka, J.; Lowther, J.; Mucha, A.; Drag, M.; Kafarski, P.; McGowan, S.; Whisstock, J. C.; Gardiner, D. L.; Dalton, J. P. *Plasmodium falciparum* neutral aminopeptidases: New targets for antimalarials. *Trends Biochem. Sci.* **2009**, *35*, 53−61.

(13) Gardiner, D. L.; Skinner-Adams, T. S.; Brown, C. L.; Andrews, K. T.; Stack, C. M.; McCarthy, J. S.; Dalton, J. P.; Trenholme, K. R. *Plasmodium falciparum*: New molecular targets with potential for antimalarial drug development. *Expert Rev. Anti-Infect. Ther.* **2009**, *7*, 1087−1098.

(14) Gavigan, C. S.; Dalton, J. P.; Bell, A. The role of aminopeptidases in haemoglobin degradation in *Plasmodium falciparum*-infected erythrocytes. *Mol. Biochem. Parasitol.* **2001**, *117*, 37−48.

(15) Gardiner, D. L.; Trenholme, K. R.; Skinner-Adams, T. S.; Stack, C. M.; Dalton, J. P. Overexpression of leucyl aminopeptidase in *Plasmodium falciparum* parasites. Target for the antimalarial activity of bestatin. *J. Biol. Chem.* **2006**, *281*, 1741−1745.

(16) Skinner-Adams, T. S.; Lowther, J.; Teuscher, F.; Stack, C. M.; Grembecka, J.; Mucha, A.; Kafarski, P.; Trenholme, K. R.; Dalton, J. P.; Gardiner, D. L. Identification of phosphinate dipeptide analog inhibitors directed against the *Plasmodium falciparum* M17 leucine aminopeptidase as lead antimalarial compounds. *J. Med. Chem.* **2007**, *50*, 6024−6031.

(17) Allary, M.; Schrevel, J.; Florent, I. Properties, stage-dependent expression and localization of *Plasmodium falciparum* M1 family zinc-aminopeptidase. *Parasitology* **2002**, *125*, 1−10.

(18) Florent, I.; Derhy, Z.; Allary, M.; Monsigny, M.; Mayer, R.; Schrevel, J. A *Plasmodium falciparum* aminopeptidase gene belonging to the M1 family of zinc-metallopeptidases is expressed in erythrocytic stages. *Mol. Biochem. Parasitol.* **1998**, *97*, 149−160.

(19) Ragheb, D.; Dalal, S.; Bompiani, K. M.; Ray, W. K.; Klemba, M. Distribution and biochemical properties of an M1-family aminopeptidase in *Plasmodium falciparum* indicate a role in vacuolar hemoglobin catabolism. *J. Biol. Chem.* **2011**, *286*, 27255−27265.

(20) Klemba, M.; Gluzman, I.; Goldberg, D. E. A *Plasmodium falciparum* dipeptidyl aminopeptidase I participates in vacuolar hemoglobin degradation. *J. Biol. Chem.* **2004**, *279*, 43000−43007.

(21) Harbut, M. B.; Velmourougane, G.; Dalal, S.; Reiss, G.; Whisstock, J. C.; Onder, O.; Brisson, D.; McGowan, S.; Klemba, M.; Greenbaum, D. C. Bestatin-based chemical biology strategy reveals distinct roles for malaria M1- and M17-family aminopeptidases. *Proc. Natl. Acad. Sci. U. S. A.* **2011**, *108*, E526−E534.

(22) Kitjaroentham, A.; Suthiphongchai, T.; Wilairat, P. Effect of metalloprotease inhibitors on invasion of red blood cell by *Plasmodium falciparum*. *Acta Trop.* **2006**, *97*, 5−9.

(23) Azimzadeh, O.; Sow, C.; Geze, M.; Nyalwidhe, J.; Florent, I. *Plasmodium falciparum* PfA-M1 aminopeptidase is trafficked via the parasitophorous vacuole and marginally delivered to the food vacuole. *Malaria J.* **2010**, *9*, 189.

(24) Flipo, M.; Florent, I.; Grellier, P.; Sergheraert, C.; Deprez-Poulain, R. Design, synthesis and antimalarial activity of novel, quinoline-based, zinc metallo-aminopeptidase inhibitors. *Bioorg. Med. Chem. Lett.* **2003**, *13*, 2659−2662.

(25) Flipo, M.; Beghyn, T.; Charton, J.; Leroux, V. A.; Deprez, B. P.; Deprez-Poulain, R. F. A library of novel hydroxamic acids targeting the metallo-protease family: Design, parallel synthesis and screening. *Bioorg. Med. Chem.* **2007**, *15*, 63−76.

(26) Flipo, M.; Beghyn, T.; Leroux, V.; Florent, I.; Deprez, B. P.; Deprez-Poulain, R. F. Novel selective inhibitors of the zinc plasmodial aminopeptidase PfA-M1 as potential antimalarial agents. *J. Med. Chem.* **2007**, *50*, 1322−1334.

(27) Cunningham, E.; Drag, M.; Kafarski, P.; Bell, A. Chemical target validation studies of aminopeptidase in malaria parasites using {alpha}-aminoalkylphosphonate and phosphonopeptide inhibitors. *Antimicrob. Agents Chemother.* **2008**, *52*, 3221−3228.

(28) Velmourougane, G.; Harbut, M. B.; Dalal, S.; McGowan, S.; Oellig, C. A.; Meinhardt, N.; Whisstock, J. C.; Klemba, M.; Greenbaum, D. C. Synthesis of new (−)-bestatin-based inhibitor libraries reveals a novel binding mode in the S1 pocket of the essential

malaria M1 metalloaminopeptidase. *J. Med. Chem.* **2011**, *54*, 1655−1666.
(29) McGowan, S.; Porter, C. J.; Lowther, J.; Stack, C. M.; Golding, S. J.; Skinner-Adams, T. S.; Trenholme, K. R.; Teuscher, F.; Donnelly, S. M.; Grembecka, J.; Mucha, A.; Kafarski, P.; DeGori, R.; Buckle, A. M.; Gardiner, D. L.; Whisstock, J. C.; Dalton, J. P. Structural basis for the inhibition of the essential *Plasmodium falciparum* M1 neutral aminopeptidase. *Proc. Natl. Acad. Sci. U. S. A.* **2009**, *106*, 2537−2542.
(30) Morgenthaler, M.; Aebi, J. D.; Grüninger, F.; Mona, D.; Wagner, B.; Kansy, M.; Diederich, F. A fluorine scan of non-peptidic inhibitors of neprilysin: Fluorophobic and fluorophilic regions in an enzyme active site. *J. Fluor. Chem.* **2008**, *129*, 852−865.
(31) Huang, Y.; Wolf, S.; Koes, D.; Popowicz, G. M.; Camacho, C. J.; Holak, T. A.; Dömling, A. Exhaustive fluorine scanning toward potent p53−Mdm2 antagonists. *ChemMedChem* **2012**, *7*, 49−52.
(32) Flipo, M.; Charton, J.; Hocine, A.; Dassonneville, S.; Deprez, B.; Deprez-Poulain, R. Hydroxamates: Relationships between structure and plasma stability. *J. Med. Chem.* **2009**, *52*, 6790−6802.
(33) O'Hagan, D. Fluorine in health care: Organofluorine containing blockbuster drugs. *J. Fluor. Chem.* **2010**, *131*, 1071−1081.
(34) Gakh, A. A.; Burnett, M. N. Extreme modulation properties of aromatic fluorine. *J. Fluor. Chem.* **2011**, *132*, 88−93.
(35) Smart, B. E. Fluorine substituent effects (on bioactivity). *J. Fluor. Chem.* **2001**, *109*, 3−11.
(36) Saleh, M.; Abbott, S.; Perron, V.; Lauzon, C.; Penney, C.; Zacharie, B. Synthesis and antimicrobial activity of 2-fluorophenyl-4,6-disubstituted [1,3,5]triazines. *Bioorg. Med. Chem. Lett.* **2010**, *20*, 945−949.
(37) Bertrand, T.; Kothe, M.; Liu, J.; Dupuy, A.; Rak, A.; Berne, P. F.; Davis, S.; Gladysheva, T.; Valtre, C.; Crenne, J. Y.; Mathieu, M. The crystal structures of TrkA and TrkB suggest key regions for achieving selective inhibition. *J. Mol. Biol.* **2012**, 439−453.
(38) Whitehead, L.; Dobler, M. R.; Radetich, B.; Zhu, Y.; Atadja, P. W.; Claiborne, T.; Grob, J. E.; McRiner, A.; Pancost, M. R.; Patnaik, A.; Shao, W.; Shultz, M.; Tichkule, R.; Tommasi, R. A.; Vash, B.; Wang, P.; Stams, T. Human HDAC isoform selectivity achieved via exploitation of the acetate release channel with structurally unique small molecule inhibitors. *Bioorg. Med. Chem.* **2011**, *19*, 4626−4634.
(39) Kassahun, K.; Farrell, K.; Abbott, F. Identification and characterization of the glutathione and *N*-acetylcysteine conjugates of (*E*)-2-propyl-2,4-pentadienoic acid, a toxic metabolite of valproic acid, in rats and humans. *Drug Metab. Dispos.* **1991**, *19*, 525−535.
(40) Hasegawa, T.; Hara, K.; Hata, S. Binding of dorzolamide and its metabolite, N-deethylated dorzolamide, to human erythrocytes in vitro. *Drug Metab. Dispos.* **1994**, *22*, 377−382.
(41) Iyer, R.; Barrese, A. A.; Parakh, S.; Parker, C. N.; Tripp, B. C. Inhibition profiling of human carbonic anhydrase II by high-throughput screening of structurally diverse, biologically active compounds. *J. Biomol. Screen.* **2006**, *11*, 782−791.
(42) Peng, S. X. Separation and identification methods for metalloproteinase inhibitors. *J. Chromatogr., B* **2001**, *764*, 59−80.